Banner appropriate to article type will appear here in typeset article

# Supplementary Information: Soft streaming – flow rectification via elastic boundaries

**Yashraj Bhosale[1], Tejaswin Parthasarathy[1], and Mattia Gazzola[1234]†**

[1]Mechanical Sciences and Engineering, University of Illinois at Urbana-Champaign, Urbana, IL 61801, USA

[2]National Center for Supercomputing Applications, University of Illinois at Urbana-Champaign, Urbana, IL 61801, USA

[3]Carl R. Woese Institute for Genomic Biology, University of Illinois at Urbana-Champaign, Urbana, IL 61801, USA

[4]Center for Artificial Intelligence Innovation, University of Illinois at Urbana-Champaign, Urbana, IL 61801, USA

(Received xx; revised xx; accepted xx)

## 1. Derivation of viscous streaming solution for elastic bodies

Here we present a detailed, step-by-step derivation of the viscous streaming solution in the case of a hyperelastic two-dimensional cylinder. At the high level the logic of our derivation is the following—we first present the problem setup with the complete set of governing equations and boundary conditions. We then non-dimensionalize them through appropriate scales, introducing the system's key non-dimensional parameters, together with their range in typical settings. We perturb the relevant fields (velocity, deformation, pressure) as an asymptotic series of powers of the non-dimensional oscillation amplitude $\epsilon$, to obtain approximations of the flow field solution at different orders. We derive the purely oscillatory solution at zeroth order $O(1)$, which reduces to a rigid cylinder immersed in a fluid governed by the unsteady Stokes equation. We then derive the next order solution $O(\epsilon)$ in two steps. First, we obtain the deformation of the elastic solid due to the zeroth order flow in the fluid phase. Next, we use this deformation to derive the necessary boundary condition for the fluid flow, thus incorporating the effect of elasticity into the rectified streaming flow solution.

This section is organized as follows: problem setup, governing equations and boundary conditions are presented in Section 1.1; their non-dimensionalization and key system-defining parameters are discussed in Section 1.2; candidate perturbation series solution and final form of the relevant equations are shown in Section 1.3; zeroth order (purely oscillatory) solution is derived in Section 1.4; finally, the first order (steady streaming) flow solution including the effects of elasticity are discussed in Section 1.6.

### 1.1. *Problem setup and governing equations*

We consider the case of a two-dimensional circular visco-hyperelastic cylinder (Fig. 1) of radius $a$ immersed in a viscous fluid, with the fluid oscillating with velocity $V(t)$ =

† Email address for correspondence: mgazzola@illinois.edu

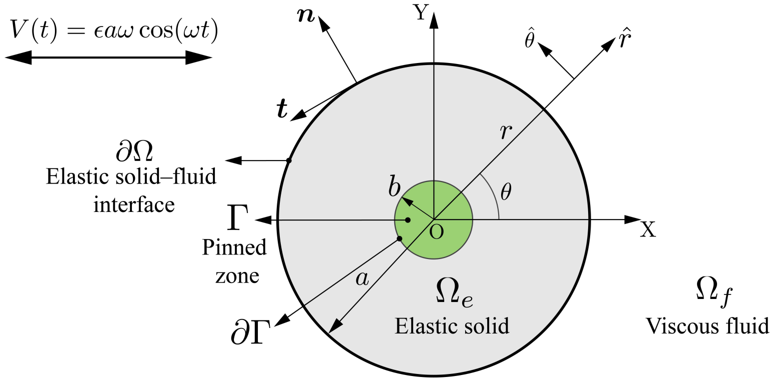


Figure 1: Problem setup. Elastic solid cylinder ($\Omega_e$) of radius $a$ with a rigid inclusion (pinned zone $\Gamma$ of radius $b$), immersed in a viscous fluid ($\Omega_f$). The cylinder is subjected to an oscillatory flow with far-field velocity $V(t) = \epsilon a\omega\cos(\omega t)$, where $\epsilon$ and $\omega$ correspond to the non-dimensional oscillation amplitude and the frequency of oscillation, respectively.

$\epsilon a\omega\cos\omega t$, where $\epsilon$, $\omega$ and $t$ represent the non-dimensional amplitude, angular frequency and time, respectively. We 'pin' the cylinder's centre using a cylindrical, rigid inclusion of radius $b$, where $b < a$, to kinematically enforce zero strain and velocities near the cylinder's centre. This pinned zone $\Gamma$ also serves the purpose of eliminating the trivial solution of the entire cylinder vibrating in-sync with the fluid (i.e. $V_{cyl}(t) = \epsilon a\omega\cos\omega t$).

We denote with $\Omega_e$ & $\partial\Omega$ the region occupied by the elastic cylinder and the boundary between the elastic solid and viscous fluid, respectively. The region occupied by the fluid is represented by $\Omega_f$. The fluid is assumed to be Newtonian, isotropic and incompressible with density $\rho_f$ and dynamic viscosity $\mu_f$.

Next, we assume that the solid is isotropic, incompressible and of constant density $\rho_e$. We assume that the solid exhibits viscoelastic Kelvin-Voigt behavior, where the elastic stresses are modeled via neo-Hookean hyperelasticity, characteristic of soft biological materials (Bower 2009). Nonetheless, as it will later become apparent, the choice of hyperelastic or viscoelastic model does not affect the general theory presented in this study.

The dynamics in the elastic and fluid phases, in the absence of body forces, is described by the Navier–Stokes (fluid) and the Cauchy (solid) momentum equations

$$
\begin{aligned}
\rho_f\left(\frac{\partial \boldsymbol{v}}{\partial t} + (\boldsymbol{v}\cdot\boldsymbol{\nabla})\boldsymbol{v}\right) &= -\nabla p + \mu_f\nabla^2\boldsymbol{v}, \quad \boldsymbol{x}\in\Omega_f \\
\rho_e\left(\frac{\partial \boldsymbol{v}}{\partial t} + (\boldsymbol{v}\cdot\boldsymbol{\nabla})\boldsymbol{v}\right) &= -\nabla p + \mu_e\nabla^2\boldsymbol{v} + \boldsymbol{\nabla}\cdot\boldsymbol{\sigma}'_{he}, \quad \boldsymbol{x}\in\Omega_e
\end{aligned}
\tag{1.1}
$$

where $p$ and $\boldsymbol{v}$ correspond to pressure and velocity fields, respectively. As a convention, the prime symbol $'$ on a tensor $\boldsymbol{A}$ denotes it is deviatoric, i.e. $\boldsymbol{A}' := \boldsymbol{A} - \frac{1}{2}tr(\boldsymbol{A})\boldsymbol{I}$, with $\boldsymbol{I}$ representing the tensor identity and $tr(\cdot)$ representing the trace operator. Thus, $\boldsymbol{\sigma}'_{he}$ corresponds to the deviatoric hyperelastic stress inside the elastic solid, which for a neo-Hookean solid is given by

$$
\boldsymbol{\sigma}'_{he} = G(\boldsymbol{F}\boldsymbol{F}^T)', \tag{1.2}
$$

where $\boldsymbol{F}$ corresponds to a finite strain measure known as the deformation gradient tensor, defined as $\boldsymbol{F} = \partial\boldsymbol{x}/\partial\boldsymbol{X}$. Here $\boldsymbol{X}$ and $\boldsymbol{x}$ correspond to the position of a material point at rest and after deformation, respectively. Alternatively, $\boldsymbol{F}$ can also be written in a more intuitive form

$\boldsymbol{F} = \boldsymbol{I} + \boldsymbol{\nabla u}$, where $\boldsymbol{u} = \boldsymbol{x} - \boldsymbol{X}$, known as the displacement field, corresponds to the relative deformation of a material point. Along with the above governing equations, incompressibility translates to the following constraint on the velocity field in the fluid phase

$$\boldsymbol{\nabla} \cdot \boldsymbol{v} = 0, \quad \boldsymbol{x} \in \Omega_f \tag{1.3}$$

and in the solid phase

$$\begin{aligned} \boldsymbol{\nabla} \cdot \boldsymbol{v} &= 0, \quad \boldsymbol{x} \in \Omega_e \\ det(\boldsymbol{F}) &= 1, \quad \boldsymbol{x} \in \Omega_e \end{aligned} \tag{1.4}$$

where $det(\cdot)$ is the determinant operator. Note that $det(\boldsymbol{F}) = 1$ follows from $\boldsymbol{\nabla} \cdot \boldsymbol{v} = 0$ (Jain *et al.* 2019) and it is not an additional constraint. Nonetheless, we recall it here as it will become useful later on.

To close the system of equations, we next derive the necessary boundary conditions, relative to the pinned zone, interfacial conditions, and far-field conditions. First, the rigid inclusion at the centre of the cylinder enforces zero velocity and strain fields over its domain $\Gamma$

$$\begin{aligned} \boldsymbol{v} &= 0, \quad \boldsymbol{x} \in \Gamma \\ \boldsymbol{u} &= 0, \quad \boldsymbol{x} \in \Gamma. \end{aligned} \tag{1.5}$$

Second, the fluid and elastic solid phases interact exclusively via boundary conditions at the fluid–elastic solid interface. This implies continuity in velocities (no-slip)

$$\boldsymbol{v}_f = \boldsymbol{v}_e, \quad \boldsymbol{x} \in \partial\Omega \tag{1.6}$$

and traction forces (normal and tangential components)

$$\begin{aligned} \boldsymbol{n} \cdot (-p_f \boldsymbol{I} + 2\mu_f \boldsymbol{D}'_f) \cdot \boldsymbol{n} &= \boldsymbol{n} \cdot (-p_e \boldsymbol{I} + 2\mu_e \boldsymbol{D}'_e + G(\boldsymbol{F}\boldsymbol{F}^T)') \cdot \boldsymbol{n}, \qquad \boldsymbol{x} \in \partial\Omega \\ \boldsymbol{n} \cdot (-p_f \boldsymbol{I} + 2\mu_f \boldsymbol{D}'_f) \cdot \boldsymbol{t} &= \boldsymbol{n} \cdot (-p_e \boldsymbol{I} + 2\mu_e \boldsymbol{D}'_e + G(\boldsymbol{F}\boldsymbol{F}^T)') \cdot \boldsymbol{t}, \qquad \boldsymbol{x} \in \partial\Omega \end{aligned} \tag{1.7}$$

where $\boldsymbol{n}$ and $\boldsymbol{t}$ denote the unit outward normal vector and tangent vector at the interface $\partial\Omega$ (Fig. 1). The subscripts $e$ and $f$ refer to elastic and fluid phases respectively. Here $\boldsymbol{D}'$ is the strain rate tensor $(\boldsymbol{\nabla v} + \boldsymbol{\nabla v}^T)/2$. Finally, the flow velocity field away from the cylinder must approach the unperturbed oscillatory flow, so that

$$\boldsymbol{v}(|\boldsymbol{x}| \to \infty) = \epsilon a \omega \cos \omega t \; \bar{i}, \quad \boldsymbol{x} \in \Omega_f \tag{1.8}$$

where $\bar{i}$ refers to the oscillation direction. This concludes the definition of our model problem and introduces all governing equations and boundary conditions necessary to its solution.

### 1.2. *Non-dimensional form and key parameters*

Next, we non-dimensionalize the governing equations and boundary conditions, followed by the identification of the system's key non-dimensional parameters, together with their range in typical viscous streaming scenarios. Following the setup of Fig. 1, we choose the characteristic scales of velocity, length and time to be $V = \epsilon a \omega$, $L = a$ and $T = 1/\omega$, respectively. We also define the density ratio as $\alpha = \rho_s/\rho_f$ and the viscosity ratio as $\beta = \mu_s/\mu_f$. Given that streaming is observed in flow regimes with low to moderate inertia (i.e. large viscous effects), we scale the hydrostatic pressure using viscous stresses, so that the pressure scale is $P = \mu_f V/L$. Non-dimensional relevant quantities and operators can then be expressed as

$$\hat{\boldsymbol{x}} = \frac{\boldsymbol{x}}{a}; \quad \hat{t} = \omega t; \quad \hat{\boldsymbol{v}} = \frac{\boldsymbol{v}}{\epsilon a \omega}; \quad \hat{\boldsymbol{\nabla}} = a \boldsymbol{\nabla}; \quad \hat{p} = \frac{p}{\mu_f \epsilon \omega}; \quad \hat{\boldsymbol{F}} = \boldsymbol{F}; \quad \hat{\boldsymbol{D}}' = \frac{\boldsymbol{D}'}{\epsilon \omega}; \quad \hat{\boldsymbol{n}} = \boldsymbol{n}; \quad \hat{\boldsymbol{t}} = \boldsymbol{t}. \tag{1.9}$$

By substituting the above quantities into Eq. (1.1), we obtain in the fluid phase

$$\left(\frac{\partial \hat{\boldsymbol{v}}}{\partial \hat{t}} + \epsilon(\hat{\boldsymbol{v}} \cdot \hat{\boldsymbol{\nabla}})\hat{\boldsymbol{v}}\right) = -\frac{\mu_f}{\rho_f a^2 \omega}\hat{\nabla}\hat{p} + \frac{\mu_f}{\rho_f a^2 \omega}\hat{\nabla^2}\hat{\boldsymbol{v}}, \quad \hat{\boldsymbol{x}} \in \Omega_f \tag{1.10}$$

and in the solid phase

$$\frac{\epsilon \rho_f a^2 \omega^2}{G}(\alpha)\left(\frac{\partial \hat{\boldsymbol{v}}}{\partial \hat{t}} + \epsilon(\hat{\boldsymbol{v}} \cdot \hat{\boldsymbol{\nabla}})\hat{\boldsymbol{v}}\right) = -\frac{\epsilon \mu_f \omega}{G}\hat{\nabla}\hat{p} + \frac{\epsilon \mu_f \omega}{G}(\beta)\hat{\nabla^2}\hat{\boldsymbol{v}} + \hat{\boldsymbol{\nabla}} \cdot (\hat{\boldsymbol{F}}\hat{\boldsymbol{F}}^T)', \quad \hat{\boldsymbol{x}} \in \Omega_e. \tag{1.11}$$

Finally, by introducing the Womersley number $M = a\sqrt{\rho_f \omega / \mu_f}$, which is the inverse of the non-dimensional Stokes layer thickness, and $\mathrm{Cau} = \epsilon \rho_f a^2 \omega^2 / G$, which is the Cauchy number and represents the ratio of inertial to elastic forces, we obtain

$$\left(\frac{\partial \hat{\boldsymbol{v}}}{\partial \hat{t}} + \epsilon(\hat{\boldsymbol{v}} \cdot \hat{\boldsymbol{\nabla}})\hat{\boldsymbol{v}}\right) = -\frac{1}{M^2}\hat{\nabla}\hat{p} + \frac{1}{M^2}\hat{\nabla^2}\hat{\boldsymbol{v}}, \quad \hat{\boldsymbol{x}} \in \Omega_f \tag{1.12}$$

and

$$\mathrm{Cau}(\alpha)\left(\frac{\partial \hat{\boldsymbol{v}}}{\partial \hat{t}} + \epsilon(\hat{\boldsymbol{v}} \cdot \hat{\boldsymbol{\nabla}})\hat{\boldsymbol{v}}\right) = -\frac{\mathrm{Cau}}{M^2}\hat{\nabla}\hat{p} + \frac{\mathrm{Cau}}{M^2}(\beta)\hat{\nabla^2}\hat{\boldsymbol{v}} + \hat{\boldsymbol{\nabla}} \cdot (\hat{\boldsymbol{F}}\hat{\boldsymbol{F}}^T)', \quad \hat{\boldsymbol{x}} \in \Omega_e. \tag{1.13}$$

Similar to the governing equations above, non-dimensionalization transforms Eq. (1.6) and Eq. (1.7) into the following non-dimensional boundary conditions

$$\hat{\boldsymbol{v}}_f = \hat{\boldsymbol{v}}_e \quad \hat{\boldsymbol{x}} \in \partial\Omega \tag{1.14}$$

$$\begin{aligned}
\hat{\boldsymbol{n}} \cdot \left(\frac{\mathrm{Cau}}{M^2}(-\hat{p}_f \boldsymbol{I} + 2\hat{\boldsymbol{D}}'_f)\right) \cdot \hat{\boldsymbol{n}} &= \hat{\boldsymbol{n}} \cdot \left(\frac{\mathrm{Cau}}{M^2}(-\hat{p}_e \boldsymbol{I} + 2(\beta)\hat{\boldsymbol{D}}'_e) + (\hat{\boldsymbol{F}}\hat{\boldsymbol{F}}^T)'\right) \cdot \hat{\boldsymbol{n}}, \qquad \hat{\boldsymbol{x}} \in \partial\Omega \\
\hat{\boldsymbol{n}} \cdot \left(\frac{\mathrm{Cau}}{M^2}(-\hat{p}_f \boldsymbol{I} + 2\hat{\boldsymbol{D}}'_f)\right) \cdot \hat{\boldsymbol{t}} &= \hat{\boldsymbol{n}} \cdot \left(\frac{\mathrm{Cau}}{M^2}(-\hat{p}_e \boldsymbol{I} + 2(\beta)\hat{\boldsymbol{D}}'_e) + (\hat{\boldsymbol{F}}\hat{\boldsymbol{F}}^T)'\right) \cdot \hat{\boldsymbol{t}}, \qquad \hat{\boldsymbol{x}} \in \partial\Omega.
\end{aligned} \tag{1.15}$$

Lastly, the incompressibility constraints of Eq. (1.3) and Eq. (1.4) and the pinned zone constraints of Eq. (1.5) remain unchanged, while the far-field condition now reads as follows

$$\hat{\boldsymbol{v}}(|\hat{\boldsymbol{x}}| \to \infty) = \cos t\, \bar{i}, \quad \hat{\boldsymbol{x}} \in \Omega_f. \tag{1.16}$$

We note that the key parameters that define the system behaviour are $\epsilon$, $M$ and Cau. We reemphasize that $\epsilon$ corresponds to the non-dimensional oscillation amplitude and for viscous streaming $\epsilon \ll 1$. The Womersley number $M$, the inverse of the non-dimensional Stokes layer thickness (or AC layer thickness $\delta_{AC}/a$) is typically $M \geqslant O(1)$ (Marmottant & Hilgenfeldt 2004; Lutz *et al.* 2006). Accordingly, here we assume $\epsilon \ll 1$ and $M = O(1)$. These assumptions have been shown to provide accurate results for boundary layer scalings and velocity decay for systems with small to moderate flow inertia (Holtsmark *et al.* 1954; Bertelsen *et al.* 1973; Lutz *et al.* 2005), which are commonly encountered in inertial microfluidics.

Lastly, the parameter Cau, known as the Cauchy number, represents the ratio of inertial to elastic forces in the system. For a rigid body $\mathrm{Cau} = 0$, while for an elastic body $\mathrm{Cau} > 0$, with $\mathrm{Cau} \ll 1$ implying a weakly elastic body. We note that, from a theoretical perspective, dealing with $\mathrm{Cau} \geqslant O(1)$ is challenging due to the highly non-linear nature of the stress-strain response in hyperelastic materials. Here, to gain theoretical insight, we assume that the cylinder is instead weakly elastic $\mathrm{Cau} \ll 1$ and in particular that $\mathrm{Cau} = \kappa\epsilon$, where $\kappa = O(1)$. This assumption simplifies the application of asymptotics/perturbation theory, allowing us to investigate the effect of body elasticity on the streaming solution in the limit of $\epsilon \to 0$, thus Cau $\rightarrow 0$. This is because the problem dependence is reduced to one small parameter $\epsilon$ (i.e. Cau and $\epsilon$ are assumed to be equally small). We postpone more generic and convoluted limits for Cau and $\epsilon$ to future studies.

Lastly, for the less significant parameters density ratio $\alpha$ and viscosity ratio $\beta$, we assume $\alpha = \mathcal{O}(1)$ and $\beta = \mathcal{O}(1)$. Nonetheless, these assumptions have negligible influence on the final streaming flow solution, as it shall become clear in the following.

### 1.3. *Perturbation series approach*

Given the above assumptions and limits, we now perturb all relevant fields (velocity, pressure, deformation and interface location) as an asymptotic series with powers of $\epsilon$ as gauge functions, valid in the limit $\epsilon \rightarrow 0$ and Cau $\rightarrow 0$. Henceforth, to simplify notation, we drop the use of $[\hat{\cdot}]$, thus assuming all quantities to be non-dimensional.

With increasing powers of $\epsilon$, we obtain higher order correction terms in the approximate solution, approaching the true problem solution in the limit $\epsilon \rightarrow 0$ and Cau $\rightarrow 0$. In this work, we aim to derive the solution at least to first order $\mathcal{O}(\epsilon)$, where streaming is known to emerge in the rigid body case. Hence, we perturb all relevant quantities to $\mathcal{O}(\epsilon)$ as shown below

$$\begin{aligned} \boldsymbol{v} &\sim \boldsymbol{v}_0 + \epsilon \boldsymbol{v}_1 + \mathcal{O}\left(\epsilon^2\right) \\ \boldsymbol{u} &\sim \boldsymbol{u}_0 + \epsilon \boldsymbol{u}_1 + \mathcal{O}\left(\epsilon^2\right) \\ \boldsymbol{n} &\sim \boldsymbol{n}_0 + \epsilon \boldsymbol{n}_1 + \mathcal{O}\left(\epsilon^2\right) \\ \boldsymbol{t} &\sim \boldsymbol{t}_0 + \epsilon \boldsymbol{t}_1 + \mathcal{O}\left(\epsilon^2\right) \\ p &\sim p_0 + \epsilon p_1 + \mathcal{O}\left(\epsilon^2\right) \\ \partial\Omega &\sim \partial\Omega_0 + \epsilon \partial\Omega_1 + \mathcal{O}\left(\epsilon^2\right) \end{aligned} \tag{1.17}$$

where the subscript (0, 1, ...) indicates the order of the solution. By substituting the above expansions into Eq. (1.12) and Eq. (1.13) we obtain the following form of the governing equations in the fluid

$$\begin{aligned} &\left(\frac{\partial(\boldsymbol{v}_0 + \epsilon \boldsymbol{v}_1 + \ldots)}{\partial t} + \epsilon((\boldsymbol{v}_0 + \epsilon \boldsymbol{v}_1 + \ldots) \cdot \boldsymbol{\nabla})(\boldsymbol{v}_0 + \epsilon \boldsymbol{v}_1 + \ldots)\right) \\ &= -\frac{1}{M^2}\nabla(p_0 + \epsilon p_1 + \ldots) + \frac{1}{M^2}\nabla^2(\boldsymbol{v}_0 + \epsilon \boldsymbol{v}_1 + \ldots), \quad \boldsymbol{x} \in \Omega_f \end{aligned} \tag{1.18}$$

and in the solid phase

$$\begin{aligned} &\kappa\epsilon(\alpha)\left(\frac{\partial(\boldsymbol{v}_0 + \epsilon \boldsymbol{v}_1 + \ldots)}{\partial t} + \epsilon((\boldsymbol{v}_0 + \epsilon \boldsymbol{v}_1 + \ldots) \cdot \boldsymbol{\nabla})(\boldsymbol{v}_0 + \epsilon \boldsymbol{v}_1 + \ldots)\right) \\ &= -\frac{\kappa\epsilon}{M^2}\nabla(p_0 + \epsilon p_1 + \ldots) + \frac{\kappa\epsilon}{M^2}(\beta)\nabla^2(\boldsymbol{v}_0 + \epsilon \boldsymbol{v}_1 + \ldots) \\ &+ \boldsymbol{\nabla} \cdot ((\boldsymbol{I} + \boldsymbol{\nabla}\boldsymbol{u}_0 + \epsilon \boldsymbol{\nabla}\boldsymbol{u}_1 + \ldots)(\boldsymbol{I} + \boldsymbol{\nabla}\boldsymbol{u}_0 + \epsilon \boldsymbol{\nabla}\boldsymbol{u}_1 + \ldots)^T)', \quad \boldsymbol{x} \in \Omega_e. \end{aligned} \tag{1.19}$$

Further, incompressibility in the fluid phase implies

$$\boldsymbol{\nabla} \cdot (\boldsymbol{v}_0 + \epsilon \boldsymbol{v}_1 + \ldots) = 0, \quad \boldsymbol{x} \in \Omega_f \tag{1.20}$$

while in the solid phase we have

$$\begin{aligned} \nabla \cdot (\boldsymbol{v}_0 + \epsilon \boldsymbol{v}_1 + \ldots) &= 0, \quad \boldsymbol{x} \in \Omega_e \\ det(\boldsymbol{I} + \nabla \boldsymbol{u}_0 + \epsilon \nabla \boldsymbol{u}_1 + \ldots) &= 1, \quad \boldsymbol{x} \in \Omega_e. \end{aligned} \tag{1.21}$$

Moving on to the boundary conditions, constraints induced by the pinned zone (Eq. (1.5)) read

$$\begin{aligned} (\boldsymbol{v}_0 + \epsilon \boldsymbol{v}_1 + \ldots) &= 0, \quad \boldsymbol{x} \in \Gamma \\ (\boldsymbol{u}_0 + \epsilon \boldsymbol{u}_1 + \ldots) &= 0, \quad \boldsymbol{x} \in \Gamma. \end{aligned} \tag{1.22}$$

Interfacial boundary conditions (Eq. (1.14) and Eq. (1.15)) follow as

$$(\boldsymbol{v}_{f,0} + \epsilon \boldsymbol{v}_{f,1} + \ldots) = (\boldsymbol{v}_{e,0} + \epsilon \boldsymbol{v}_{e,1} + \ldots) \quad \boldsymbol{x} \in \partial\Omega \tag{1.23}$$

$$\begin{aligned} &(\boldsymbol{n}_0 + \epsilon \boldsymbol{n}_1 + \ldots) \cdot \left( \frac{\epsilon \kappa}{M^2} (-(p_{f,0} + \epsilon p_{f,1} + \ldots)\boldsymbol{I} + 2(\boldsymbol{D}'_{f,0} + \epsilon \boldsymbol{D}'_{f,1} + \ldots)) \right) \cdot (\boldsymbol{n}_0 + \epsilon \boldsymbol{n}_1 + \ldots) \\ &\quad = (\boldsymbol{n}_0 + \epsilon \boldsymbol{n}_1 + \ldots) \cdot \left( \frac{\epsilon \kappa}{M^2} (-(p_{e,0} + \epsilon p_{e,1} + \ldots)\boldsymbol{I} + 2(\beta)(\boldsymbol{D}'_{e,0} + \epsilon \boldsymbol{D}'_{e,1} + \ldots)) \right. \\ &\quad \left. + ((\boldsymbol{I} + \nabla \boldsymbol{u}_0 + \epsilon \nabla \boldsymbol{u}_1 + \ldots)(\boldsymbol{I} + \nabla \boldsymbol{u}_0 + \epsilon \nabla \boldsymbol{u}_1 + \ldots)^T)' \right) \cdot (\boldsymbol{n}_0 + \epsilon \boldsymbol{n}_1 + \ldots) \;\; \boldsymbol{x} \in \partial\Omega \end{aligned} \tag{1.24}$$

$$\begin{aligned} &(\boldsymbol{n}_0 + \epsilon \boldsymbol{n}_1 + \ldots) \cdot \left( \frac{\epsilon \kappa}{M^2} (-(p_{f,0} + \epsilon p_{f,1} + \ldots)\boldsymbol{I} + 2(\boldsymbol{D}'_{f,0} + \epsilon \boldsymbol{D}'_{f,1} + \ldots)) \right) \cdot (\boldsymbol{t}_0 + \epsilon \boldsymbol{t}_1 + \ldots) \\ &\quad = (\boldsymbol{n}_0 + \epsilon \boldsymbol{n}_1 + \ldots) \cdot \left( \frac{\epsilon \kappa}{M^2} (-(p_{e,0} + \epsilon p_{e,1} + \ldots)\boldsymbol{I} + 2(\beta)(\boldsymbol{D}'_{e,0} + \epsilon \boldsymbol{D}'_{e,1} + \ldots)) \right. \\ &\quad \left. + ((\boldsymbol{I} + \nabla \boldsymbol{u}_0 + \epsilon \nabla \boldsymbol{u}_1 + \ldots)(\boldsymbol{I} + \nabla \boldsymbol{u}_0 + \epsilon \nabla \boldsymbol{u}_1 + \ldots)^T)' \right) \cdot (\boldsymbol{t}_0 + \epsilon \boldsymbol{t}_1 + \ldots) \;\; \boldsymbol{x} \in \partial\Omega. \end{aligned} \tag{1.25}$$

Lastly, the far-field condition reads

$$(\boldsymbol{v}_0 + \epsilon \boldsymbol{v}_1 + \ldots)(|\boldsymbol{x}| \to \infty) = \cos t \; \bar{i}, \quad \boldsymbol{x} \in \Omega_f. \tag{1.26}$$

Before proceeding, we briefly describe the key steps we will follow to derive the flow field field solutions at different orders. Given the pinned zone constraints and governing equations in the solid phase, we first derive the solution for the deformation of the elastic body. From this we compute the motion of the solid–fluid interface. This, in turn, provides us with the appropriate boundary conditions to solve the governing equations in the fluid phase. Below we describe this procedure for $O(1)$.

### 1.4. *Zeroth order $O(1)$ governing equations and boundary conditions*

We begin with the derivation of the zeroth order $O(1)$ solution. Zeroth order equations are obtained by recovering the $O(1)$ terms from the governing equations Eq. (1.18) and Eq. (1.19) and boundary conditions Eqs. (1.23) to (1.26). Alternatively, the zeroth order equations can be obtained by setting $\epsilon = 0$. First, the governing equations for the fluid phase (Eqs. (1.18) and (1.20)) reduce to the unsteady Stokes equations

$$M^2 \frac{\partial \boldsymbol{v}_0}{\partial t} = -\nabla p_0 + \nabla^2 \boldsymbol{v}_0, \quad \nabla \cdot \boldsymbol{v}_0 = 0, \quad \boldsymbol{x} \in \Omega_f \tag{1.27}$$

while in the elastic solid phase, the governing equations (Eqs. (1.19) and (1.21)) reduce to

$$\nabla \cdot ((\boldsymbol{I} + \nabla \boldsymbol{u}_0)(\boldsymbol{I} + \nabla \boldsymbol{u}_0)^T)' = 0, \quad \nabla \cdot \boldsymbol{v}_0 = 0, \quad \boldsymbol{x} \in \Omega_e. \tag{1.28}$$

To solve the above equations, the fluid $\Omega_f$ and elastic $\Omega_e$ domains (hence their common boundary $\partial\Omega$) need to be determined (hence their common boundary $\partial\Omega$), which we do by considering the zeroth order boundary conditions. We start from the pinned zone constraints of Eq. (1.22), which reduce to

$$\begin{aligned} \boldsymbol{v}_0 &= 0, \quad \boldsymbol{x} \in \Gamma \\ \boldsymbol{u}_0 &= 0, \quad \boldsymbol{x} \in \Gamma. \end{aligned} \tag{1.29}$$

Since Cau = 0 (implied by Cau = $\kappa\epsilon$) the elastic solid is actually rigid at zeroth order so that the direct solution of Eq. (1.28), with the constraints of Eq. (1.29), corresponds to the fixed rigid cylinder

$$\begin{gathered} \boldsymbol{v}_0 = 0, \quad \boldsymbol{u}_0 = 0, \quad \boldsymbol{x} \in \partial\Omega_0 \\ \partial\Omega_0 := r = 1 \end{gathered} \tag{1.30}$$

where $\partial\Omega_0$ is the boundary at the non-dimensional radius $r = 1$. Because of the no-slip boundary condition for the velocity field, and continuity in pressure fields (Angot *et al.* (1999)), we have

$$\begin{aligned} \boldsymbol{v}_{f,0} &= 0, && \boldsymbol{x} \in \partial\Omega_0 \\ p_{f,0} &= p_{e,0}, && \boldsymbol{x} \in \partial\Omega_0 \end{aligned} \tag{1.31}$$

while the far-field condition of Eq. (1.26) reads

$$\boldsymbol{v}_0(|\boldsymbol{x}| \to \infty) = \cos t\, \bar{i}, \quad \boldsymbol{x} \in \Omega_f. \tag{1.32}$$

## 1.5. *Zeroth order $O(1)$ solution in cylindrical coordinates*

To solve the above system of equations, we introduce the more convenient cylindrical coordinate system $(r, \theta)$, with $r$ being the radial coordinate and $\theta$ the angular coordinate. With the origin of the coordinate system at the center of the cylinder, and oscillation direction $\bar{i}$ corresponding to $\theta = 0$, the no-slip boundary condition Eq. (1.31) and the far-field condition Eq. (1.32) can be written as

$$\begin{aligned} v_{0,r}|_{r=1} &= 0 \\ v_{0,\theta}|_{r=1} &= 0 \\ v_{0,r}|_{r\to\infty} &= \cos\theta\ \cos t \\ v_{0,\theta}|_{r\to\infty} &= -\sin\theta\ \cos t. \end{aligned} \tag{1.33}$$

For the zeroth order solution derivation, we next consider the streamfunction $\psi$ form of Eq. (1.27)

$$M^2 \frac{\partial \nabla^2 \psi_0}{\partial t} = \nabla^4 \psi_0, \quad r \geqslant 1 \tag{1.34}$$

where $\boldsymbol{v}_0 = \boldsymbol{\nabla} \times \psi_0$. The solution of the above equation was derived by Holtsmark *et al.* (1954) and can be written as

$$\psi_0 = \sin\theta \left(0.5r + 0.5\frac{H_2(m)}{rH_0(m)} - \frac{H_1(mr)}{mH_0(m)}\right) e^{-it} + c.c., \quad r \geqslant 1 \tag{1.35}$$

where $i = \sqrt{-1}$ and $m = \sqrt{i}M$. Here, $H_i$ and $c.c.$ refer to the $i^{th}$ order Hankel function of first kind and complex conjugate, respectively. Consequently, the velocity field $\boldsymbol{v}_0$ is given by

$$\begin{aligned} v_{0,r} &= \frac{1}{r}\frac{\partial\psi_0}{\partial\theta} &&= \cos\theta \left(0.5 + 0.5\frac{H_2(m)}{r^2H_0(m)} - 0.5\frac{H_0(mr)}{H_0(m)} - 0.5\frac{H_2(mr)}{H_0(m)}\right) e^{-it} + c.c. \\ v_{0,\theta} &= -\frac{\partial\psi_0}{\partial r} &&= \sin\theta \left(-0.5 + 0.5\frac{H_2(m)}{r^2H_0(m)} + 0.5\frac{H_0(mr)}{H_0(m)} - 0.5\frac{H_2(mr)}{H_0(m)}\right) e^{-it} + c.c., \ r \geqslant 1 \end{aligned} \tag{1.36}$$

where we have used the identities

$$2i\frac{H_i(mr)}{mr} = H_{i-1}(mr) + H_{i+1}(mr)$$
$$2H_i'(mr) = H_{i-1}(mr) - H_{i+1}(mr)$$

where $i$ is the order of the Hankel function. As seen from Eq. (1.36), the zeroth order velocity field $\boldsymbol{v}_0$ in the fluid is purely oscillatory, and hence no steady streaming is observed at $O(1)$ (Holtsmark *et al.* 1954; Bertelsen *et al.* 1973). Additionally, since at zeroth order Cau = 0, no effects of elasticity on the flow field manifest. As such, we then proceed to the next order of approximation $O(\epsilon)$, where we expect elasticity to affect the steady streaming solution.

### 1.6. *First order $O(\epsilon)$ governing equations and boundary conditions*

The first order governing equations are obtained by recovering the $O(\epsilon)$ terms from Eq. (1.18) and Eq. (1.19). In the fluid phase (Eq. (1.18)) we recover the inhomogeneous unsteady Stokes equation

$$M^2\frac{\partial \boldsymbol{v}_1}{\partial t} + M^2(\boldsymbol{v}_0\cdot\boldsymbol{\nabla})\boldsymbol{v}_0 = -\nabla p_1 + \nabla^2\boldsymbol{v}_1, \quad \boldsymbol{x}\in\Omega_f \tag{1.37}$$

while in the solid phase Eq. (1.19), we have

$$\kappa(\alpha)\left(\frac{\partial \boldsymbol{v}_0}{\partial t}\right) = -\frac{\kappa}{M^2}\nabla p_0 + \frac{\kappa}{M^2}(\beta)\nabla^2\boldsymbol{v}_0 + \boldsymbol{\nabla}\cdot(\boldsymbol{\nabla}\boldsymbol{u}_1 + (\boldsymbol{\nabla}\boldsymbol{u}_1)^T)', \quad \boldsymbol{x}\in\Omega_e. \tag{1.38}$$

We then substitute Eq. (1.30) in Eq. (1.38) to obtain

$$\kappa\nabla p_0 = M^2\boldsymbol{\nabla}\cdot(\boldsymbol{\nabla}\boldsymbol{u}_1 + (\boldsymbol{\nabla}\boldsymbol{u}_1)^T)', \quad \boldsymbol{x}\in\Omega_e. \tag{1.39}$$

To simplify Eq. (1.39), we note that the incompressibility constraint Eq. (1.21) reduces to the following constraint at $O(\epsilon)$

$$det(\boldsymbol{I} + \epsilon\boldsymbol{\nabla}\boldsymbol{u}_1) = 1, \quad \boldsymbol{x}\in\Omega_e. \tag{1.40}$$

Using the following identity valid in two dimensions

$$det(\boldsymbol{A}+\boldsymbol{B}) = det(\boldsymbol{A}) + det(\boldsymbol{B}) + det(\boldsymbol{A})\cdot tr(\boldsymbol{A}^{-1}\boldsymbol{B}),$$

with $\boldsymbol{A} = \boldsymbol{I},\ det(\boldsymbol{A}) = 1,\ \boldsymbol{B} = \epsilon\boldsymbol{\nabla}\boldsymbol{u}_1$ the constraint further reduces to

$$\epsilon\, tr(\boldsymbol{\nabla}\boldsymbol{u}_1) + \epsilon^2 det(\boldsymbol{\nabla}\boldsymbol{u}_1) = 0$$

which, at $O(\epsilon)$, simplifies to

$$tr(\boldsymbol{\nabla}\boldsymbol{u}_1) = \boldsymbol{\nabla}\cdot\boldsymbol{u}_1 = 0, \quad \boldsymbol{x}\in\Omega_e \tag{1.41}$$

thus simplifying Eq. (1.39) into

$$\kappa\nabla p_0 = M^2\nabla^2\boldsymbol{u}_1, \quad \boldsymbol{x}\in\Omega_e. \tag{1.42}$$

The above equation physically represents the zeroth order fluid flow ($\kappa\nabla p_0$ term) deforming the weakly elastic solid ($\boldsymbol{u}_1$). As pointed out previously, Eq. (1.39) shows how the choice of hyperelasticity model does not affect equations at $O(\epsilon)$. Indeed, the higher order non-linear terms in the stress strain response drop out, due to linearization. Additionally, the effects of density and viscosity ratios ($\alpha$ and $\beta$) as well as the effect of solid viscosity have also disappeared at this order.

To solve the governing equations above, similar to the procedure at the previous order, we consider the boundary conditions at $O(\epsilon)$, starting from the pinned zone constraints of

Eq. (1.22), which at $\mathcal{O}(\epsilon)$ read as

$$\begin{aligned} \boldsymbol{v}_1 &= 0, \quad \boldsymbol{x} \in \Gamma \\ \boldsymbol{u}_1 &= 0, \quad \boldsymbol{x} \in \Gamma. \end{aligned} \tag{1.43}$$

Next, we consider the solid–fluid interfacial stress boundary conditions of Eq. (1.24) and Eq. (1.25), which when evaluated at $\mathcal{O}(\epsilon)$ accurate interface $\partial\Omega_0 + \epsilon\partial\Omega_1$, with substitution of Eq. (1.30) give

$$\begin{aligned}
\boldsymbol{n} \cdot \left( \frac{\mathrm{Cau}}{M^2}(-p_f \boldsymbol{I} + 2\boldsymbol{D}'_f) \right) \cdot \boldsymbol{n} \Big|_{\partial\Omega} &= \epsilon \boldsymbol{n}_0 \cdot \left( \frac{\kappa}{M^2}(-p_{f,0}\boldsymbol{I} + 2\boldsymbol{D}'_{f,0}) \right) \cdot \boldsymbol{n}_0 \Big|_{\partial\Omega_0 + \epsilon\partial\Omega_1} + \mathcal{O}\left(\epsilon^2\right) \\
&= \epsilon \boldsymbol{n}_0 \cdot \left( \frac{\kappa}{M^2}(-p_{f,0}\boldsymbol{I} + 2\boldsymbol{D}'_{f,0}) \right) \cdot \boldsymbol{n}_0 \Big|_{\partial\Omega_0} + \mathcal{O}\left(\epsilon^2\right) \\
&= \boldsymbol{n} \cdot \left( \frac{\mathrm{Cau}}{M^2}(-p_e \boldsymbol{I} + 2(\beta)\boldsymbol{D}'_e) + (\boldsymbol{F}\boldsymbol{F}^T)' \right) \cdot \boldsymbol{n} \Big|_{\partial\Omega} \\
&= \epsilon \boldsymbol{n}_0 \cdot \left( \frac{\kappa}{M^2}(-p_{e,0}\boldsymbol{I} + 2(\beta)\boldsymbol{D}'_{e,0}) + (\nabla \boldsymbol{u}_1 + (\nabla \boldsymbol{u}_1)^T)' \right) \cdot \boldsymbol{n}_0 \Big|_{\partial\Omega_0 + \epsilon\partial\Omega_1} \\
&+ \mathcal{O}\left(\epsilon^2\right) \\
&= \epsilon \boldsymbol{n}_0 \cdot \left( \frac{\kappa}{M^2}(-p_{e,0}\boldsymbol{I} + 2(\beta)\boldsymbol{D}'_{e,0}) + (\nabla \boldsymbol{u}_1 + (\nabla \boldsymbol{u}_1)^T)' \right) \cdot \boldsymbol{n}_0 \Big|_{\partial\Omega_0} \\
&+ \mathcal{O}\left(\epsilon^2\right) \\
\boldsymbol{n} \cdot \left( \frac{\mathrm{Cau}}{M^2}(-p_f \boldsymbol{I} + 2\boldsymbol{D}'_f) \right) \cdot \boldsymbol{t} \Big|_{\partial\Omega} &= \epsilon \boldsymbol{n}_0 \cdot \left( \frac{\kappa}{M^2}(-p_{f,0}\boldsymbol{I} + 2\boldsymbol{D}'_{f,0}) \right) \cdot \boldsymbol{t}_0 \Big|_{\partial\Omega_0 + \epsilon\partial\Omega_1} + \mathcal{O}\left(\epsilon^2\right) \\
&= \epsilon \boldsymbol{n}_0 \cdot \left( \frac{\kappa}{M^2}(-p_{f,0}\boldsymbol{I} + 2\boldsymbol{D}'_{f,0}) \right) \cdot \boldsymbol{t}_0 \Big|_{\partial\Omega_0} + \mathcal{O}\left(\epsilon^2\right) \\
&= \boldsymbol{n} \cdot \left( \frac{\mathrm{Cau}}{M^2}(-p_e \boldsymbol{I} + 2(\beta)\boldsymbol{D}'_e) + (\boldsymbol{F}\boldsymbol{F}^T)' \right) \cdot \boldsymbol{t} \Big|_{\partial\Omega} \\
&= \epsilon \boldsymbol{n}_0 \cdot \left( \frac{\kappa}{M^2}(-p_{e,0}\boldsymbol{I} + 2(\beta)\boldsymbol{D}'_{e,0}) + (\nabla \boldsymbol{u}_1 + (\nabla \boldsymbol{u}_1)^T)' \right) \cdot \boldsymbol{t}_0 \Big|_{\partial\Omega_0 + \epsilon\partial\Omega_1} \\
&+ \mathcal{O}\left(\epsilon^2\right) \\
&= \epsilon \boldsymbol{n}_0 \cdot \left( \frac{\kappa}{M^2}(-p_{e,0}\boldsymbol{I} + 2(\beta)\boldsymbol{D}'_{e,0}) + (\nabla \boldsymbol{u}_1 + (\nabla \boldsymbol{u}_1)^T)' \right) \cdot \boldsymbol{t}_0 \Big|_{\partial\Omega_0} \\
&+ \mathcal{O}\left(\epsilon^2\right).
\end{aligned} \tag{1.44}$$

Retention of $\mathcal{O}(\epsilon)$ terms in Eq. (1.44) gives us

$$\begin{aligned}
\boldsymbol{n}_0 \cdot \left( \frac{\kappa}{M^2}(-p_{f,0}\boldsymbol{I} + 2\boldsymbol{D}'_{f,0}) \right) \cdot \boldsymbol{n}_0 &= \boldsymbol{n}_0 \cdot \left( \frac{\kappa}{M^2}(-p_{e,0}\boldsymbol{I} + 2(\beta)\boldsymbol{D}'_{e,0}) + (\nabla \boldsymbol{u}_1 + (\nabla \boldsymbol{u}_1)^T)' \right) \cdot \boldsymbol{n}_0 \\
\boldsymbol{n}_0 \cdot \left( \frac{\kappa}{M^2}(-p_{f,0}\boldsymbol{I} + 2\boldsymbol{D}'_{f,0}) \right) \cdot \boldsymbol{t}_0 &= \boldsymbol{n}_0 \cdot \left( \frac{\kappa}{M^2}(-p_{e,0}\boldsymbol{I} + 2(\beta)\boldsymbol{D}'_{e,0}) + (\nabla \boldsymbol{u}_1 + (\nabla \boldsymbol{u}_1)^T)' \right) \cdot \boldsymbol{t}_0, \\
&\boldsymbol{x} \in \partial\Omega_0.
\end{aligned} \tag{1.45}$$

Here, $\boldsymbol{n}_0$ and $\boldsymbol{t}_0$ refer to the normal and tangent vectors at the zeroth order, that is the rigid body interface $\partial\Omega_0$. These conditions (Eq. (1.45)) can be simplified using Eq. (1.30) and

Eq. (1.31) to obtain

$$
\begin{aligned}
\boldsymbol{n}_0 \cdot \left(2\boldsymbol{D}'_{f,0}\right) \cdot \boldsymbol{n}_0 &= \boldsymbol{n}_0 \cdot \left(\frac{M^2}{\kappa}(\boldsymbol{\nabla u}_1 + (\boldsymbol{\nabla u}_1)^T)'\right) \cdot \boldsymbol{n}_0, \qquad \boldsymbol{x} \in \partial\Omega_0 \\
\boldsymbol{n}_0 \cdot \left(2\boldsymbol{D}'_{f,0}\right) \cdot \boldsymbol{t}_0 &= \boldsymbol{n}_0 \cdot \left(\frac{M^2}{\kappa}(\boldsymbol{\nabla u}_1 + (\boldsymbol{\nabla u}_1)^T)'\right) \cdot \boldsymbol{t}_0, \qquad \boldsymbol{x} \in \partial\Omega_0.
\end{aligned}
\tag{1.46}
$$

## 1.7. *First order $O(\epsilon)$ solution in cylindrical coordinates*

With $O(\epsilon)$ governing equations and boundary conditions in hand, we proceed as before to derive their analytical solution. We start by deriving an expression for the displacement field $\boldsymbol{u}_1$ inside the solid. We define $\zeta = b/a$ as the non-dimensional radius of the pinned zone. Adopting a cylindrical coordinate system, the solid pinned zone constraints of Eq. (1.43) read as

$$
\begin{aligned}
u_{1,r}|_{r=\zeta} &= 0 \\
u_{1,\theta}|_{r=\zeta} &= 0
\end{aligned}
\tag{1.47}
$$

while the solid–fluid interfacial stress boundary conditions of Eq. (1.46) become

$$
\begin{aligned}
\left.\frac{\partial v_{0,r}}{\partial r}\right|_{r=1} &= \frac{M^2}{\kappa}\left.\frac{\partial u_{1,r}}{\partial r}\right|_{r=1} \\
\left.\left(\frac{1}{r}\frac{\partial v_{0,r}}{\partial \theta} + \frac{\partial v_{0,\theta}}{\partial r} - \frac{v_{0,\theta}}{r}\right)\right|_{r=1} &= \frac{M^2}{\kappa}\left.\left(\frac{1}{r}\frac{\partial u_{1,r}}{\partial \theta} + \frac{\partial u_{1,\theta}}{\partial r} - \frac{u_{1,\theta}}{r}\right)\right|_{r=1}.
\end{aligned}
\tag{1.48}
$$

We note that Eq. (1.41) implies that $\boldsymbol{u}_1$ is divergence free, which allows the definition of a streamfunction-equivalent strain function $\psi_{e,1}$ where $\boldsymbol{u}_1 = \boldsymbol{\nabla} \times \psi_{e,1}$. Taking the curl ($\boldsymbol{\nabla}\times$) of Eq. (1.42), and expressing $\boldsymbol{u}_1$ in terms of $\psi_{e,1}$, we obtain the following homogeneous fourth order biharmonic equation

$$
\nabla^4 \psi_{e,1} = 0, \quad \boldsymbol{x} \in \Omega_e \tag{1.49}
$$

with the pinned zone constraints (Eq. (1.47)) becoming

$$
\begin{aligned}
\left.\frac{1}{r}\frac{\partial \psi_{e,1}}{\partial \theta}\right|_{r=\zeta} &= 0 \\
\left.\frac{\partial \psi_{e,1}}{\partial r}\right|_{r=\zeta} &= 0.
\end{aligned}
\tag{1.50}
$$

Next, the boundary conditions of Eq. (1.48), with forcing terms (i.e. previous order terms) moved to the RHS, become

$$
\begin{aligned}
\left.\frac{\partial}{\partial r}\left(\frac{1}{r}\frac{\partial \psi_{e,1}}{\partial \theta}\right)\right|_{r=1} &= \frac{\kappa}{M^2}\left.\frac{\partial v_{0,r}}{\partial r}\right|_{r=1} \\
\left.\left(\frac{1}{r^2}\frac{\partial^2 \psi_{e,1}}{\partial \theta^2} - \frac{\partial^2 \psi_{e,1}}{\partial r^2} + \frac{1}{r}\frac{\partial \psi_{e,1}}{\partial r}\right)\right|_{r=1} &= \frac{\kappa}{M^2}\left.\left(\frac{1}{r}\frac{\partial v_{0,r}}{\partial \theta} + \frac{\partial v_{0,\theta}}{\partial r} - \frac{v_{0,\theta}}{r}\right)\right|_{r=1}.
\end{aligned}
\tag{1.51}
$$

The RHS of Eq. (1.51) can be evaluated using Eq. (1.36) and the recurrence properties of Hankel functions, yielding

$$
\begin{aligned}
\left.\frac{\partial v_{0,r}}{\partial r}\right|_{r=1} &= \cos\theta\left(-\frac{H_2(m)}{r^3 H_0(m)} + \frac{H_1(mr)}{mr^2 H_0(m)} + 0.5\frac{H_2(mr)}{rH_0(m)} - 0.5\frac{H_0(mr)}{rH_0(m)}\right)e^{-it} + c.c.\Big|_{r=1} = 0\\
\left.\frac{\partial v_{0,r}}{\partial \theta}\right|_{r=1} &= -\sin\theta\left(0.5 + 0.5\frac{H_2(m)}{r^2 H_0(m)} - \frac{H_1(mr)}{mrH_0(m)}\right)e^{-it} + c.c.\Big|_{r=1} = 0\\
\left.\frac{\partial v_{0,\theta}}{\partial r}\right|_{r=1} &= \sin\theta\left(-\frac{H_2(m)}{r^3 H_0(m)} + \frac{H_2(mr)}{rH_0(m)} - \frac{mH_1(mr)}{H_0(m)}\right)e^{-it} + c.c.\Big|_{r=1}\\
&= \sin\theta\, F(m)\, e^{-it} + c.c.
\end{aligned}
\tag{1.52}
$$

Here, $F(m)$ expresses in compact form the bracketed terms. Using Eq. (1.52), conditions of Eq. (1.51) simplify to

$$
\begin{aligned}
\left.\frac{\partial}{\partial r}\left(\frac{1}{r}\frac{\partial \psi_{e,1}}{\partial \theta}\right)\right|_{r=1} &= 0\\
\left.\left(\frac{1}{r^2}\frac{\partial^2 \psi_{e,1}}{\partial \theta^2} - \frac{\partial^2 \psi_{e,1}}{\partial r^2} + \frac{1}{r}\frac{\partial \psi_{e,1}}{\partial r}\right)\right|_{r=1} &= \frac{\kappa}{M^2}\sin\theta\, F(m)\, e^{-it} + c.c.
\end{aligned}
\tag{1.53}
$$

Now we have expressions for the four boundary conditions (pinned zone constraints - Eq. (1.50); solid–fluid interfacial stress boundary conditions - Eq. (1.53)) necessary to solve the elastic solid fourth order differential equation (Eq. (1.49)). Based on the form of the boundary conditions in Eq. (1.53), we choose for the homogeneous biharmonic equation (Eq. (1.49)) the candidate general solution (Michell 1899)

$$
\psi_{e,1} = \frac{\kappa}{M^2}\sin\theta\left(c_1 r + \frac{c_2}{r} + c_3 r^3 + c_4 r\, ln(r)\right)F(m)\, e^{-it} + c.c. \tag{1.54}
$$

where $c_1$, $c_2$, $c_3$ and $c_4$ are constants that are determined from the 4 boundary conditions given by Eq. (1.50) and Eq. (1.53)

$$
\begin{aligned}
c_1 + \frac{c_2}{\zeta^2} + c_3\zeta^2 + c_4\, ln(\zeta) &= 0\\
c_1 - \frac{c_2}{\zeta^2} + 3c_3\zeta^2 + c_4(ln(\zeta)+1) &= 0\\
-2c_2 + 2c_3 + c_4 &= 0\\
-4(c_2 + c_3) &= 1.
\end{aligned}
\tag{1.55}
$$

Solving the above linear system of equations yields

$$
\begin{aligned}
c_1 &= 0.5\frac{(\zeta^2+1)ln(\zeta)}{(\zeta^2-1)} - 0.25\\
c_2 &= -0.25\frac{\zeta^2}{\zeta^2-1}\\
c_3 &= \frac{0.25}{\zeta^2-1}\\
c_4 &= -0.5\frac{(\zeta^2+1)}{\zeta^2-1}.
\end{aligned}
\tag{1.56}
$$

Having determined the strain function $\psi_{e,1}$, we proceed to evaluate $\boldsymbol{u}_1 = \boldsymbol{\nabla}\times\psi_{e,1}$ at the cylinder surface ($r = 1$), which will eventually feed into the solution of the fluid phase, through the no-slip condition. The interfacial displacement $\boldsymbol{u}_1$, accurate up to $\mathcal{O}(\epsilon)$ is then given by

$$\begin{aligned} u_{1,r} = \frac{1}{r}\frac{\partial \psi_{e,1}}{\partial \theta}\bigg|_{r=1} &= \frac{\kappa}{M^2}\cos\theta\left(c_1 + \frac{c_2}{r^2} + c_3 r^2 + c_4\, ln(r)\right) F(m)\, e^{-it} + c.c.\bigg|_{r=1} \\ &= \frac{\kappa}{M^2}\cos\theta\, G_1(\zeta)\, F(m)\, e^{-it} + c.c. \\ u_{1,\theta} = -\frac{\partial \psi_{e,1}}{\partial r}\bigg|_{r=1} &= -\frac{\kappa}{M^2}\sin\theta\left(c_1 - \frac{c_2}{r^2} + 3c_3 r^2 + c_4 (ln(r)+1)\right) F(m)\, e^{-it} + c.c.\bigg|_{r=1} \\ &= -\frac{\kappa}{M^2}\sin\theta\, G_2(\zeta)\, F(m)\, e^{-it} + c.c. \end{aligned} \tag{1.57}$$

with $G_1(\zeta)$ and $G_2(\zeta)$ as the compact notation for the bracketed terms.

We now have all the conditions required to evalute the solution in the fluid phase at $\mathcal{O}(\epsilon)$. We recall that the governing equations in the fluid phase (Eq. (1.37)) can be written in streamfunction form, which at $\mathcal{O}(\epsilon)$ read

$$M^2\frac{\partial \nabla^2 \psi_1}{\partial t} + M^2\left(\left(\boldsymbol{v}_0\cdot\boldsymbol{\nabla}\right)\nabla^2\psi_0\right) = \nabla^4\psi_1, \quad r \geqslant 1 \tag{1.58}$$

where $\boldsymbol{v}_1 = \boldsymbol{\nabla}\times\psi_1$. In order to solve for $\psi_1$, we first focus on the forcing term $M^2\left(\left(\boldsymbol{v}_0\cdot\boldsymbol{\nabla}\right)\nabla^2\psi_0\right)$, which using Eq. (1.36), similar to the derivation in Holtsmark *et al.* (1954), can be expressed as

$$M^2\left(\left(\boldsymbol{v}_0\cdot\boldsymbol{\nabla}\right)\nabla^2\psi_0\right) = \sin 2\theta\left(\rho(r) + \Omega(r)e^{-2it} + \Omega^*(r)e^{2it}\right) \tag{1.59}$$

where

$$\rho(r) = -\frac{M^4}{2}\, Im\left[\frac{H_2(mr)}{H_0(m)} + \frac{H_2(m)H_0^*(mr)}{H_0^2(m)r^2} + 2\frac{H_0(mr)H_2^*(mr)}{H_0^2(m)}\right]. \tag{1.60}$$

Here superscript $^*$ indicates complex conjugate, while $Im[\cdot]$ stands for the imaginary part. The terms $\sin 2\theta\,\Omega(r)e^{2it}$ and $\sin 2\theta\,\Omega(r)e^{-2it}$ correspond to higher order oscillatory forcing terms, which generate oscillatory unsteady corrections to the first order flow. The term $\sin 2\theta\ \rho(r)$ is, instead, real, steady, time-independent and is the one responsible for the streaming flow that emerges in the case of a rigid cylider, as demonstrated previously in Holtsmark *et al.* (1954). Since we are interested in steady streaming flow, we consider the time averaged form of Eq. (1.58) (i.e. we drop the time derivative), yielding

$$\nabla^4\langle\psi_1\rangle = \sin 2\theta\,\rho(r), \quad r \geqslant 1 \tag{1.61}$$

where $\langle\cdot\rangle$ stands for a time averaged field. To solve the above equation in the fluid phase, we recall the necessary no-slip boundary condition given in Eq. (1.23), that needs to be enforced at the elastic solid–fluid interface, deformed by the zeroth order flow. Based on Eq. (1.57), we note that $r = 1 + \epsilon u_{1,r}$ corresponds to an $\mathcal{O}(\epsilon)$ accurate expression for the location of the deforming interface. The no-slip condition of Eq. (1.23) can then be written as

$$\begin{aligned} v_{f,r}\big|_{\partial\Omega} = v_{f,r}\big|_{r=1+\epsilon u_{1,r}} + \mathcal{O}\left(\epsilon^2\right) \quad &= v_{e,r}\big|_{\partial\Omega} \quad = v_{e,r}\big|_{r=1+\epsilon u_{1,r}} + \mathcal{O}\left(\epsilon^2\right) \\ v_{f,\theta}\big|_{\partial\Omega} = v_{f,\theta}\big|_{r=1+\epsilon u_{1,r}} + \mathcal{O}\left(\epsilon^2\right) \quad &= v_{e,\theta}\big|_{\partial\Omega} \quad = v_{e,\theta}\big|_{r=1+\epsilon u_{1,r}} + \mathcal{O}\left(\epsilon^2\right) \end{aligned} \tag{1.62}$$

We recall that the subscripts $e$ and $f$ refer to the interfacial field values from the elastic solid and fluid perspective, respectively. The RHS of Eq. (1.62) is the deformation velocity of the elastic solid interface, which can be computed from the deformation field $\boldsymbol{u}$ of Eq. (1.57) as

$$\begin{aligned}
v_{e,r}\big|_{\partial\Omega} &= \left.\frac{\partial u_r}{\partial t}\right|_{r=1+\epsilon u_{1,r}} + O\left(\epsilon^2\right) = \left.\frac{\partial(\epsilon u_{1,r} + O\left(\epsilon^2\right))}{\partial t}\right|_{r=1+\epsilon u_{1,r}} + O\left(\epsilon^2\right) \\
&= \left.\frac{\partial(\epsilon u_{1,r} + O\left(\epsilon^2\right))}{\partial t}\right|_{r=1} + \epsilon u_{1,r}\left.\frac{\partial^2(\epsilon u_{1,r} + O\left(\epsilon^2\right))}{\partial r \partial t}\right|_{r=1} + O\left(\epsilon^2\right) \\
&= \epsilon \left.\frac{\partial u_{1,r}}{\partial t}\right|_{r=1} + O\left(\epsilon^2\right) \\
&= -\epsilon i \frac{\kappa}{M^2} \cos\theta \, G_1(\zeta)\, F(m)\, e^{-it} + c.c. + O\left(\epsilon^2\right) \\
v_{e,\theta}\big|_{\partial\Omega} &= \left.\frac{\partial u_\theta}{\partial t}\right|_{r=1+\epsilon u_{1,r}} + O\left(\epsilon^2\right) = \left.\frac{\partial(\epsilon u_{1,\theta} + O\left(\epsilon^2\right))}{\partial t}\right|_{r=1+\epsilon u_{1,r}} + O\left(\epsilon^2\right) \\
&= \left.\frac{\partial(\epsilon u_{1,\theta} + O\left(\epsilon^2\right))}{\partial t}\right|_{r=1} + \epsilon u_{1,r}\left.\frac{\partial^2(\epsilon u_{1,\theta} + O\left(\epsilon^2\right))}{\partial r \partial t}\right|_{r=1} + O\left(\epsilon^2\right) \\
&= \epsilon \left.\frac{\partial u_{1,\theta}}{\partial t}\right|_{r=1} + O\left(\epsilon^2\right) \\
&= -\epsilon i \frac{\kappa}{M^2} \sin\theta \, G_2(\zeta)\, F(m)\, e^{-it} + c.c. + O\left(\epsilon^2\right).
\end{aligned} \tag{1.63}$$

We note that at zeroth order the deformation field is zero ($u_{0,r} = u_{0,\theta} = 0$), hence $u_r = \epsilon u_{1,r} + O\left(\epsilon^2\right)$ and $u_\theta = \epsilon u_{1,\theta} + O\left(\epsilon^2\right)$. There are now two ways to enforce the no-slip condition of Eq. (1.62) to the fluid. First, we can adopt a moving coordinate system attached to the moving interface, and enforce the no-slip condition on a fixed surface in that frame of reference. Second, we can maintain the fixed coordinate system with origin at the cylinder center, and enforce the no-slip condition on a moving interface. Since the use of moving coordinates presents technical complications in the time averaging process eventually needed for streaming, as pointed out in Longuet-Higgins (1998), we adopt the latter approach. Additionally, we can replace the boundary flow velocity $v_{f,r}|_{r=1+\epsilon u_{1,r}}$ and $v_{f,\theta}|_{r=1+\epsilon u_{1,r}}$ on the temporally moving interface $r = 1+\epsilon u_{1,r}$ with the velocity that the flow would need to see on the fixed interface $r = 1$ to respond equivalently. This boundary condition transfer can be achieved by Taylor expanding $v_{f,r}|_{r=1+\epsilon u_{1,r}}$ and $v_{f,\theta}|_{r=1+\epsilon u_{1,r}}$ about $r = 1$ (Longuet-Higgins 1998)

$$\begin{aligned}
v_{f,r}|_{\partial\Omega} = v_{f,r}|_{r=1+\epsilon u_{1,r}} + O\left(\epsilon^2\right) &= \left.\left(v_{f,r} + \frac{\partial v_{f,r}}{\partial r}(\epsilon u_{1,r} + O\left(\epsilon^2\right))\right)\right|_{r=1} + O\left(\epsilon^2\right) \\
&= \left.\left(v_{f,r} + \epsilon \frac{\partial v_{f,r}}{\partial r} u_{1,r}\right)\right|_{r=1} + O\left(\epsilon^2\right) \\
v_{f,\theta}|_{\partial\Omega} = v_{f,\theta}|_{r=1+\epsilon u_{1,r}} + O\left(\epsilon^2\right) &= \left.\left(v_{f,\theta} + \frac{\partial v_{f,\theta}}{\partial r}(\epsilon u_{1,r} + O\left(\epsilon^2\right))\right)\right|_{r=1} + O\left(\epsilon^2\right) \\
&= \left.\left(v_{f,\theta} + \epsilon \frac{\partial v_{f,\theta}}{\partial r} u_{1,r}\right)\right|_{r=1} + O\left(\epsilon^2\right).
\end{aligned} \tag{1.64}$$

Here onwards, to avoid subscript clutter, we drop the subscript $f$ and all references of the velocity field $\boldsymbol{v}$ now correspond to the velocity in the fluid phase. By combining Eqs. (1.62), (1.63) and (1.64), followed by substitution of the asymptotic series for fluid velocity $\boldsymbol{v} =$

$\boldsymbol{v}_0 + \epsilon \boldsymbol{v}_1 + O\left(\epsilon^2\right)$ and retention of $O(\epsilon)$ terms, we obtain

$$\begin{aligned}\left.\left(v_{1,r} + \frac{\partial v_{0,r}}{\partial r} u_{1,r}\right)\right|_{r=1} &= -i\frac{\kappa}{M^2}\cos\theta\, G_1(\zeta)\, F(m)\, e^{-it} + c.c.\\ \left.\left(v_{1,\theta} + \frac{\partial v_{0,\theta}}{\partial r} u_{1,r}\right)\right|_{r=1} &= -i\frac{\kappa}{M^2}\sin\theta\, G_2(\zeta)\, F(m)\, e^{-it} + c.c.\end{aligned} \tag{1.65}$$

The first term on LHS of the equation above ($\boldsymbol{v}_1|_{r=1}$), which is currently unknown, corresponds to the first order no-slip velocity that the fluid flow experiences at the zeroth order boundary $r = 1$ due to the boundary condition transfer. The second term on the LHS, which represents the correction generated due to the Taylor expansion, can be evaluated using Eq. (1.52) and Eq. (1.57) as

$$\begin{aligned}\left.\left(\frac{\partial v_{0,r}}{\partial r} u_{1,r}\right)\right|_{r=1} &= 0\\ \left.\left(\frac{\partial v_{0,\theta}}{\partial r} u_{1,r}\right)\right|_{r=1} &= \frac{\kappa}{M^2}\sin 2\theta\, \left(G_1(\zeta)F(m)F^*(m) + \phi(r)e^{-2it} + \phi^*(r)e^{2it}\right).\end{aligned} \tag{1.66}$$

Since we are interested in the effect of elasticity on steady streaming flow, we consider the time averaged form of the no-slip condition of Eq. (1.65), which using Eq. (1.66) reduces to

$$\begin{aligned}\langle v_{1,r}\rangle\big|_{r=1} &= 0\\ \langle v_{1,\theta}\rangle\big|_{r=1} &= -\frac{\kappa}{M^2}\sin 2\theta\, G_1(\zeta)F(m)F^*(m).\end{aligned} \tag{1.67}$$

Equation (1.67) tells us that an oscillatory no-slip velocity imposed on a moving interface ($r = 1 + \epsilon u_{1,r}$) can be equivalently seen as a rectified slip different from zero ($\langle v_{1,\theta}\rangle|_{r=1} \neq 0$) at the zeroth order, fixed interface $r = 1$. Such rectified slip velocities are also seen in the case of streaming flow generation due to axisymmetric pulsating bubbles (Longuet-Higgins 1998; Spelman & Lauga 2017). In our case this slip, which is non-zero only for a deformable elastic body, modifies the well-known steady streaming flow generated due to the Reynolds stress term ($\sin 2\theta\ \rho(r)$, RHS of Eq. (1.61)) induced by the rigid cylinder counterpart. We remark that this slip is independent of the non-linear inertial advection term in Navier–Stokes equations, and hence can generate streaming even in the Stokes limit, unlike the case of rigid bodies. Finally to derive the effect of this steady slip on streaming flow, we consider the streamfunction version of the time averaged no-slip condition Eq. (1.67)

$$\begin{aligned}\left.\frac{1}{r}\frac{\partial\langle\psi_1\rangle}{\partial\theta}\right|_{r=1} &= 0\\ \left.\frac{\partial\langle\psi_1\rangle}{\partial r}\right|_{r=1} &= \frac{\kappa}{M^2}\sin 2\theta\, G_1(\zeta)F(m)F^*(m)\end{aligned} \tag{1.68}$$

where $\psi_1 = \boldsymbol{\nabla}\times\boldsymbol{v}_1$. Similarly, the time averaged far-field conditions, stemming from Eq. (1.26), read

$$\begin{aligned}\left.\frac{1}{r}\frac{\partial\langle\psi_1\rangle}{\partial\theta}\right|_{r\to\infty} &= 0\\ \left.\frac{\partial\langle\psi_1\rangle}{\partial r}\right|_{r=\to\infty} &= 0.\end{aligned} \tag{1.69}$$

Finally, with the time averaged flow of equation Eq. (1.61) and the necessary boundary conditions of Eq. (1.68) and Eq. (1.69) in hand, the steady streaming flow solution for a weakly elastic cylinder can be computed, yielding

$$\langle \psi_1 \rangle = \sin 2\theta \;\; [\Theta(r) + \Lambda(r)] \tag{1.70}$$

where $\Theta(r)$ is the classical rigid body contribution, derived first in Holtsmark *et al.* (1954) and given by

$$\begin{aligned}\Theta(r) = &-\frac{r^4}{48}\int_r^\infty \frac{\rho(\tau)}{\tau}\,\mathrm{d}\tau + \frac{r^2}{16}\int_r^\infty \tau\rho(\tau)\,\mathrm{d}\tau \\ &+ \frac{1}{16}\left(\int_1^r \tau^3\rho(\tau)\,\mathrm{d}\tau + \int_1^\infty \frac{\rho(\tau)}{\tau}\,\mathrm{d}\tau - 2\int_1^\infty \tau\rho(\tau)\,\mathrm{d}\tau\right) \\ &+ \frac{1}{r^2}\left(-\frac{1}{48}\int_1^r \tau^5\rho(\tau)\,\mathrm{d}\tau - \frac{1}{24}\int_1^\infty \frac{\rho(\tau)}{\tau}\,\mathrm{d}\tau + \frac{1}{16}\int_1^\infty \tau\rho(\tau)\,\mathrm{d}\tau\right)\end{aligned} \tag{1.71}$$

and whose asymptotic nature (previously derived in Holtsmark *et al.* (1954)) is given by

$$\begin{aligned}\Theta(\infty) &= \frac{1}{16}\int_1^\infty \frac{(\tau^2-1)^2}{\tau}\rho(\tau)\,\mathrm{d}\tau \\ \frac{d\Theta}{dr}(\infty) &= 0\end{aligned} \tag{1.72}$$

Next, $\Lambda(r)$ is the new elasticity effect modification given by

$$\Lambda(r) = 0.5\frac{\kappa}{M^2}\,G_1(\zeta)F(m)F^*(m)\left(1-\frac{1}{r^2}\right) \tag{1.73}$$

and whose asymptotic nature is given by

$$\begin{aligned}\Lambda(\infty) &= 0.5\frac{\kappa}{M^2}\,G_1(\zeta)F(m)F^*(m) \\ \frac{d\Lambda}{dr}(\infty) &= 0\end{aligned} \tag{1.74}$$

where $G_1(\zeta)$ and $F(m)$ are expanded here for convenience

$$\begin{aligned}G_1(\zeta) &= 0.5\left(\frac{(\zeta^2+1)ln(\zeta)}{\zeta^2-1} - 1\right) \\ F(m) &= -\frac{mH_1(m)}{H_0(m)}\end{aligned} \tag{1.75}$$

This concludes the detailed, step-by-step derivation of the viscous streaming solution for the case of a hyperelastic two-dimensional cylinder.

## 2. Rationale for $\mathcal{O}\,(\mathrm{Cau}) = \mathcal{O}\,(\epsilon)$ assumption

In this section, we provide rationale for the assumption $\mathcal{O}\,(\mathrm{Cau}) = \mathcal{O}\,(\epsilon)$ employed in this study. A more general expansion, whereby Cau is not tied to $\epsilon$, would ultimately lead to our same main conclusions, within the limits of linear elasticity. However, we note that our results apply to viscoelastic materials as well, provided that $\mathcal{O}\,(\mathrm{Cau}) = \mathcal{O}\,(\epsilon)$. Indeed, with this assumption, the solid viscosity and the non-linear elasticity terms are of order higher than the streaming flow order, and thus drop out. On the other hand, without this assumption (or further system knowledge), it is not possible to determine the relative order of the non-linear elasticity terms with respect to the streaming flow order, thus preventing linearisation and conclusive asymptotic analysis. This argument is expanded in more mathematical detail at point 3 below.

Nonetheless, we wish to emphasize that our simplifying assumption does *not* come with much loss of practical generality. In fact, for realistic systems that may exhibit soft streaming (see Section 6), it is reasonable to expect that small oscillation amplitudes ($\epsilon$) are accompanied by weak elastic responses (Cau). This is because large values of Cau relative to $\epsilon$ may correspond to unrealistic materials and applications. For example, in our setup, assuming $\epsilon \sim O\left(10^{-1}\right)$, a value of Cau $\sim O\left(10^{-1}\right)$ corresponds to a very soft biological tissue ($G \sim$ kPa (Liu *et al.* 2015)), with larger values of Cau implying material properties not commonly found in nature, or of little engineering relevance. Therefore, without much loss of practical generality, it intuitively makes physical sense to us to tie Cau and $\epsilon$.

Based on these considerations, we believe our approach strikes a reasonable balance between mathematical simplicity and practical relevance, as summarized more formally below:

(i) In the case of viscous streaming, slaving Cau to $\epsilon$ reduces the number of perturbation parameters from two ($\epsilon$ and Cau) to one ($\epsilon$), and the number of perturbation orders to be considered from a minimum of three ($O(1)$, $O(\epsilon)$ and $O(\mathrm{Cau})$) to two ($O(1)$ and $O(\epsilon)$), thus simplifying the presentation and application of asymptotic theory.

(ii) A generic perturbation involving two parameters ($\epsilon$ and Cau) leads to the appearance of cross-terms such as $O(\epsilon\mathrm{Cau})$ or $O\left(\epsilon\mathrm{Cau}^2\right)$, which make the tracking and ordering of different terms in the expansion more involved, ultimately resulting in a derivation that can be distracting.

(iii) For a generic expansion analysis, it is critical to know the relative magnitudes of $\epsilon$ and Cau, in order to match and arrange the powers of these parameters in the right order. For instance, if $\epsilon \ll \mathrm{Cau}$, then $\epsilon^2 \ll \mathrm{Cau}^2$ or $\epsilon^2 \ll \epsilon\mathrm{Cau}$, however if the former ($\epsilon \ll \mathrm{Cau}$) is not known, we do not have enough information to arrange and match the higher order terms. A similar ordering issue can arise in the case of our setup, when considering the appearance of the solid viscosity and nonlinear elasticity terms. In fact, if Cau is chosen to be a different expansion parameter from $\epsilon$ in the asymptotic analysis, it can be shown that the solid viscosity and nonlinear elasticity terms now appear at $O\left(\mathrm{Cau}^2\right)$. However if no information is available regarding the relative magnitudes of $\epsilon$ and Cau, it is not possible to determine if the $O\left(\mathrm{Cau}^2\right)$ terms are higher order with respect to the $O(\epsilon)$ streaming flow. This issue prevents linearisation of the equations and conclusive asymptotic analysis. Instead, our assumption of $O(\epsilon) = O(\mathrm{Cau})$ resolves this issue since $O\left(\mathrm{Cau}^2\right) = O\left(\epsilon^2\right)$, implying that the solid viscosity and nonlinear elasticity terms are indeed higher order and thus drop out at the $O(\epsilon)$ streaming flow, transforming the analysis into a linear elasticity model analysis.

## 3. Stokes drift correction

The final result of Eq. 3.20 in the main text represents the Eulerian streamfunction for the steady streaming flow. However, fluid particles do not precisely follow these streamlines because of Stokes drift. This implies that true pathlines of fluid particles, i.e. the Lagrangian streamlines, require the computation of the Stokes drift to correct the Eulerian counterparts. In this section, we present a brief derivation of the Stokes drift correction, based on Raney *et al.* (1954) and Bertelsen *et al.* (1973), concluding with the final explicit form employed in this study.

Let $\boldsymbol{V}$ be the true (Lagrangian) velocity of a fluid particle. The velocity of the particle can then be expressed as a function of the Eulerian velocity flow field $\boldsymbol{v}$

$$\boldsymbol{V}(t) = \boldsymbol{v}(x_0 + \int_0^t \boldsymbol{V} d\tau,\ t) \tag{3.1}$$

where $t$ and $x_0$ correspond to the time and the location of particle at $t = 0$, respectively. Since the displacement of the particle about $x_0$ over one cycle is small, we can Taylor expand the particle velocity about $x_0$

$$\boldsymbol{V}(t) = \boldsymbol{v}(x_0, t) + \int_0^t \boldsymbol{V} d\tau \cdot \nabla \boldsymbol{v}(x_0, t) + O\left(\left(\int_0^t \boldsymbol{V} d\tau\right)^2\right). \tag{3.2}$$

Denoting $\boldsymbol{V}(t)$ by $\boldsymbol{V}$, $\boldsymbol{v}(x_0, t)$ by $\boldsymbol{v}$, and non-dimensionalising time $\hat{t} = t\omega$ and velocity $\hat{\boldsymbol{v}} = \boldsymbol{v}/\epsilon a \omega$ yields

$$\hat{\boldsymbol{V}} = \hat{\boldsymbol{v}} + \epsilon \int_0^t \hat{\boldsymbol{V}} d\tau \cdot \nabla \hat{\boldsymbol{v}} + O\left(\epsilon^2\right). \tag{3.3}$$

Henceforth, to simplify notation, we drop the use of $[\hat{\cdot}]$, thus assuming all quantities to be non-dimensional. We next perturb the particles velocity $\boldsymbol{V}$ and Eulerian velocity field $\boldsymbol{v}$ to $O(\epsilon)$, and then substitute in the equation above to obtain

$$\boldsymbol{V}_0 + \epsilon \boldsymbol{V}_1 + O\left(\epsilon^2\right) = \boldsymbol{v}_0 + \epsilon \boldsymbol{v}_1 + \epsilon \int_0^t \boldsymbol{V}_0 d\tau \cdot \nabla \boldsymbol{v}_0 + O\left(\epsilon^2\right). \tag{3.4}$$

At zeroth order $O(1)$, Eq. (3.4) reduces to

$$\boldsymbol{V}_0 = \boldsymbol{v}_0. \tag{3.5}$$

Thus to the zeroth order approximation, the Lagrangian velocity of the particle is the same as the Eulerian velocity field. At first order $O(\epsilon)$, with substitution of Eq. (3.5), Eq. (3.4) reduces to

$$\boldsymbol{V}_1 = \boldsymbol{v}_1 + \int_0^t \boldsymbol{v}_0 d\tau \cdot \nabla \boldsymbol{v}_0. \tag{3.6}$$

Since we are interested in steady streaming flow, we consider the time averaged form of Eq. (3.6) (i.e. we drop the time derivative), yielding

$$\langle \boldsymbol{V}_1 \rangle = \langle \boldsymbol{v}_1 \rangle + \langle \int_0^t \boldsymbol{v}_0 d\tau \cdot \nabla \boldsymbol{v}_0 \rangle. \tag{3.7}$$

Following Raney *et al.* (1954), Eq. (3.7) can be expressed in streamfunction form as

$$\langle \Psi_1 \rangle = \langle \psi_1 \rangle + \frac{1}{2} \nabla \times \langle \boldsymbol{v}_0 \times \int_0^t \boldsymbol{v}_0 d\tau \rangle. \tag{3.8}$$

As seen from Eq. (3.8), the Lagrangian steady streamfunction $\langle \Psi_1 \rangle$ can thus be expressed as the sum of the Eulerian steady streamfunction $\langle \psi_1 \rangle$ (Eq. 3.20 of main text) and the Stokes drift correction (last term on RHS). The explicit form of the Stokes drift term, as previously computed in Raney *et al.* (1954) is then given by

$$\frac{1}{2} \nabla \times \langle \boldsymbol{v}_0 \times \int_0^t \boldsymbol{v}_0 d\tau \rangle = \sin 2\theta\, \beta(r), \quad r \geqslant 1 \tag{3.9}$$

where

$$\beta(r) = \frac{1}{2} \mathrm{Im} \left[ \frac{H_2(mr)}{H_0(m)} + \frac{H_0(mr) H_2^*(mr)}{H_0(m) H_0^*(m)} + \frac{H_0^*(mr) H_2(m)}{H_0(m) H_0^*(m) r^2} - \frac{H_2(m)}{H_0(m) r^2} \right] \tag{3.10}$$

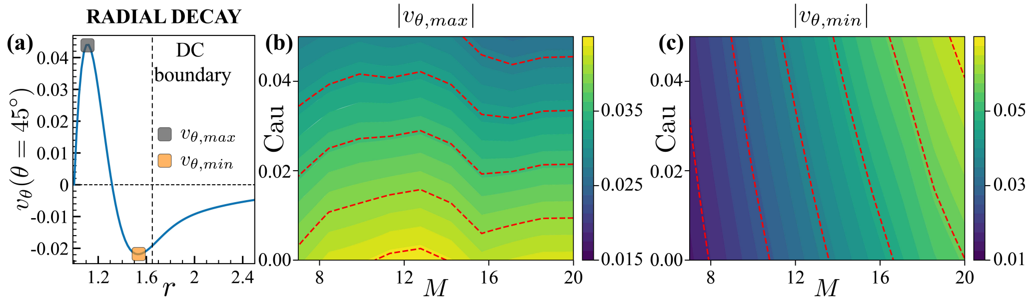


Figure 2: Effect of elasticity on streaming flow strength. (a) Radial variation of tangential Eulerian velocity $v_\theta$ along $\theta = 45°$ for $M = 10$ and Cau = 0 (rigid limit). Grey and orange markers correspond to the maximum ($v_{\theta,max}$) and minimum ($v_{\theta,min}$) velocities, respectively. (b, c) Heat-maps tracking $|v_{\theta,max}|$ and $|v_{\theta,min}|$ as functions of $M$ and Cau. Red dashed lines are iso-contours.

Here, $H_i$, $^*$, $m$ and Im$[\cdot]$ refer to the $i^{th}$ order Hankel function of first kind, complex conjugate, Womersley number and the imaginary part, respectively.

This concludes the derivation of the Stokes drift correction, in the case of steady streaming flow from a cylinder.

## 4. Effect of elasticity on flow strength

In this section, we present how variations in flow inertia ($M$) and cylinder elasticity (Cau) affect the flow strength of the resulting streaming field. Following classical streaming literature (Bertelsen *et al.* (1973)), we characterize the flow strength via the Eulerian velocity along $\theta = 45°$. Since the radial component of the velocity is $v_r = 0$ along $\theta = 45°$, we can equivalently characterise the flow strength via the tangential velocity $v_\theta$. Figure 2a (reported below) shows a typical variation of $v_\theta(\theta = 45°)$ for $M = 10$ and Cau = 0 (rigid limit). To characterise flow strength consistently, in Fig. 2b,c we track maximum ($v_{\theta,max}$, grey marker, Fig. 2a) and minimum ($v_{\theta,min}$, orange marker, Fig. 2a) velocities within the DC layer as functions of $M$ and Cau. As seen in Fig. 2(b), $|v_{\theta,max}|$ decreases with an increase in cylinder elasticity (Cau), while is approximately independent of the flow inertia $M$ (given the near horizontal red iso-contours). In Fig. 2(c), instead, $|v_{\theta,min}|$ increases with both $M$ and Cau. The above analysis provides then a compact rulebook to manipulate streaming flow strength, via variations in flow inertia ($M$) and cylinder elasticity (Cau).

## 5. Effect of pinned zone radius on streaming flow

In this section, we present the effects of varying the pinned zone radius $\zeta$ of a soft circular cylinder, on the emergent streaming flow. We first consider the elasticity-based streaming modification term $\Lambda(r)$, and specifically the prefactor $G_1(\zeta)$, which captures the $\zeta$-dependence of $\Lambda(r)$. Figure 3(a) presents the variation of $G_1(\zeta)$ with $\zeta$, where $G_1(\zeta)$ is observed to decrease with increasing $\zeta$. As $\zeta \to 1$, $G_1(\zeta)$ is seen to approach zero. This behaviour is expected since $\zeta \to 1$ implies pinning the entire cylinder, rendering the cylinder rigid and thus with no body elasticity contribution to streaming. On the other hand, as $\zeta \to 0$, a singularity is observed for $G_1(\zeta) \to \infty$. This is because it is physically unrealistic to "pin" the soft cylinder and enforce the no-slip condition in a region of zero thickness. Then, for a realistic range of pinned zone radii $\zeta$, theory predicts that decreasing the pinned zone radius $\zeta$ leads to an increase in the elastic contribution to streaming (Fig. 3a), as intuitively expected.

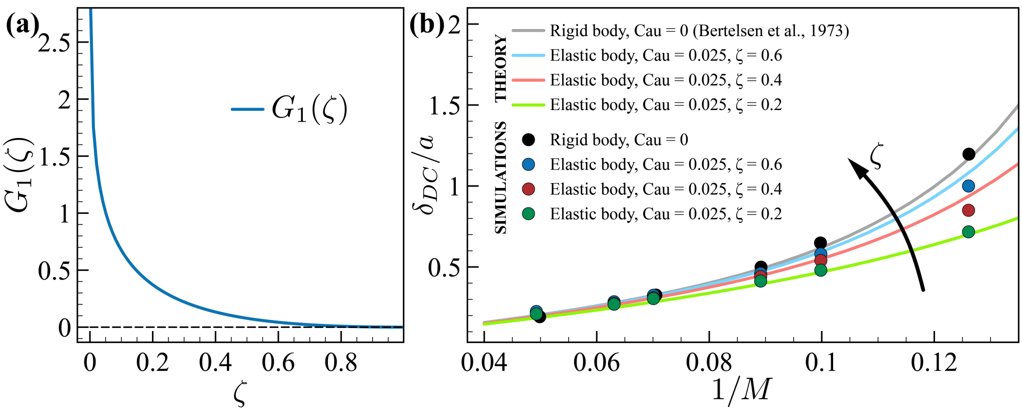


Figure 3: Effect of pinned zone radius on streaming flow. (a) Prefactor $G_1(\zeta)$, which captures the $\zeta$-dependence of the elasticity-based streaming modification term $\Lambda(r)$ versus pinned zone radius $\zeta$. (b) Normalized DC boundary layer thickness $\delta_{DC}/a$ versus the inverse of Womersley number $(1/M)$ from theory (solid lines) and simulations (circles), for rigid cylinder (Cau = 0) and soft cylinder (Cau = 0.025) with varying pinned zone radius $\zeta$.

We next proceed to validate the above theoretical predictions by comparing against results from numerical simulations. With body softness (Cau = 0.025) fixed, we vary the pinned zone radius $\zeta$ and observe its effect on streaming, characterized via the normalised DC layer thickness ($\delta_{DC}/a$). Figure 3(b) presents variation of $\delta_{DC}/a$ with the Womersley number $(1/M)$, for different values of pinned zone radius $\zeta$. Additionally, we plot the DC layer scaling for the rigid cylinder Cau = 0 (equivalently $\zeta = 1$) for reference, in Fig. 3(b). Figure 3(b) reveals a decrease in $\delta_{DC}$ with decrease in $\zeta$ across all flow regimes $M$, although this contraction is more pronounced for regimes of lower inertia (higher $1/M$). These theoretical predictions (solid lines) are confirmed by simulations (circles) across $M$. Thus, the body pinned zone radius $\zeta$ is an additional parameter that can be tuned, to rationally modulate streaming flow topologies via elasticity.

## 6. Equivalent experimental parameters

Here, we report the range of realistic experimental parameters, equivalent to the values of $M$, $\epsilon$ and Cau considered in the main text, for which body elasticity significantly affects streaming. The non-dimensional quantities ($M$, $\epsilon$ and Cau) and corresponding experimental parameter ranges are tabulated in Table 1. For streaming setup properties that include fluid density $\rho_f$, angular oscillation frequency $\omega$, fluid kinematic viscosity $\nu$ and cylinder radius $a$, we assume ranges typically employed in streaming applications (Lutz *et al.* 2005, 2006; Vishwanathan & Juarez 2019; Bhosale *et al.* 2021). Then, we derive ranges for the shear modulus $G$ of the body, showcased in the last row of Table 1. As seen from Table 1, the shear modulus ($G$) range corresponds to materials that can be realistically employed in microfluidic settings, from soft biological tissues (Liu *et al.* 2015) to common polymeric materials such as Polydimethylsiloxane (PDMS) (Lötters *et al.* 1997; Wang *et al.* 2014). We conclude that within the range of experimental parameters shown in Table 1, body elasticity can be realistically used to significantly modulate streaming flows.

| Parameter | Value range |
|---|---|
| | Non-dimensional quantities |
| $M$ | $\mathcal{O}(10)$ |
| $\epsilon$ | $\mathcal{O}\left(10^{-1}\right)$ |
| Cau | $\mathcal{O}\left(10^{-1}\right)$ |
| | Equivalent experimental quantities |
| $\rho_f$ | $\mathcal{O}\left(10^{3}\right)$ $\mathrm{kg \cdot m^{-3}}$ (Lutz *et al.* 2005; Vishwanathan & Juarez 2019; Bhosale *et al.* 2021) |
| $\nu$ | $\mathcal{O}\left(10^{-6}\right)$ $\mathrm{m^2 \cdot s^{-1}}$ (Lutz *et al.* 2005; Vishwanathan & Juarez 2019; Bhosale *et al.* 2021) |
| $a$ | $\mathcal{O}\left(10^{-3}\right)$ m (Lutz *et al.* 2005; Vishwanathan & Juarez 2019; Bhosale *et al.* 2021) |
| $\omega$ | $\mathcal{O}\left(10^{3}\right) - \mathcal{O}\left(10^{4}\right)$ $\mathrm{rad \cdot s^{-1}}$ (Lutz *et al.* 2005; Vishwanathan & Juarez 2019; Bhosale *et al.* 2021) |
| $G$ | $\mathcal{O}(1) - \mathcal{O}\left(10^{2}\right)$ kPa |

Table 1: Range of realistic experimental parameters for which body elasticity significantly affects streaming.

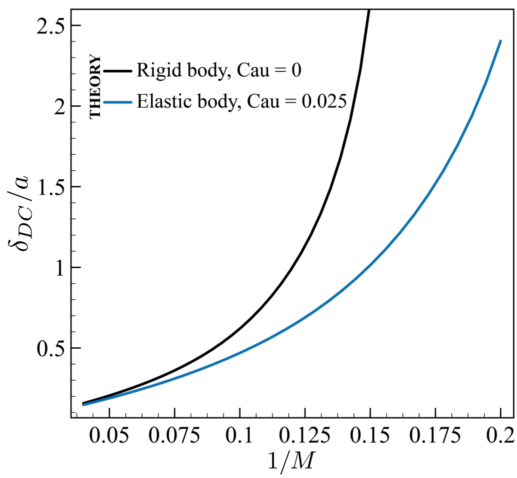


Figure 4: Normalized DC layer thickness $\delta_{DC}/a$ vs. inverse of Womersley number ($1/M$) from theory, for rigid (Cau = 0) and soft (Cau = 0.025) cylinders.

## 7. Behavior of $\delta_{DC}$ with $M$ in the limit $M \to \mathcal{O}(1)$

To investigate the behavior of $\delta_{DC}$ with $M$ for a soft cylinder, in the low inertia limit i.e. for $M \to \mathcal{O}(1)$, we extend the range of $M$ considered in the main text (Fig. 2d), and present the corresponding theoretically predicted DC layer thickness $\delta_{DC}/a$ values in Fig. 4. As it can be seen, approach to divergence is observed for Cau $> 0$, although at values of $M$ lower than those of the rigid cylinder limit. This is expected since, for Cau $> 0$, the rigid body contribution $\Theta(r)$ is the same as in classic streaming and will diverge, with the elasticity contribution $\Lambda(r)$ only shifting the curve.

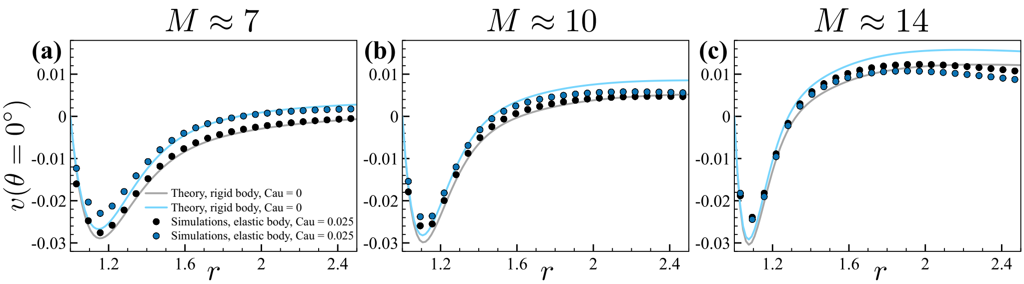


Figure 5: Radial decay of time-averaged velocity magnitude along $\theta = 0°$, from theory (lines) and simulations (scatter points), for rigid (Cau = 0, black) and soft (Cau = 0.025, blue) cylinders, with varying flow conditions (a) $M = 7$, (b) $M = 10$ and (a) $M = 14$, respectively.

## 8. Velocity decay with variation of $M$

In this section, we extend the validation of our asymptotic theory to streaming flow magnitudes across different flow conditions ($M$). We do this by plotting the radially-varying time-averaged velocity at $\theta = 0°$ for varying flow conditions $M$, in Fig. 5(a-c). We plot our theoretical predictions as solid lines, for rigid (Cau = 0, black) and soft (Cau = 0.025, blue) cylinders, upon which we overlay simulation results as scatter points. These curves display agreement for the rigid and the soft cylinder considered, across a range of $M$ values, thus providing further validation for our theory.

REFERENCES


Angot, Philippe, Bruneau, Charles-Henri & Fabrie, Pierre 1999 A penalization method to take into account obstacles in incompressible viscous flows. *Numerische Mathematik* **81** (4), 497–520.

Bertelsen, A, Svardal, Aslak & Tjøtta, Sigve 1973 Nonlinear streaming effects associated with oscillating cylinders. *Journal of Fluid Mechanics* **59** (3), 493–511.

Bhosale, Yashraj, Vishwanathan, Giridar, Parthasarathy, Tejaswin, Juarez, Gabriel & Gazzola, Mattia 2021 Multi-curvature viscous streaming: flow topology and particle manipulation. *arXiv preprint arXiv:2111.07184* .

Bower, Allan F 2009 *Applied mechanics of solids*. CRC press.

Holtsmark, J, Johnsen, I, Sikkeland, To & Skavlem, S 1954 Boundary layer flow near a cylindrical obstacle in an oscillating, incompressible fluid. *The journal of the acoustical society of America* **26** (1), 26–39.

Jain, Suhas S, Kamrin, Ken & Mani, Ali 2019 A conservative and non-dissipative eulerian formulation for the simulation of soft solids in fluids. *Journal of Computational Physics* **399**, 108922.

Liu, Juan, Zheng, Huaiyuan, Poh, Patrina SP, Machens, Hans-Günther & Schilling, Arndt F 2015 Hydrogels for engineering of perfusable vascular networks. *International journal of molecular sciences* **16** (7), 15997–16016.

Longuet-Higgins, Michael S 1998 Viscous streaming from an oscillating spherical bubble. *Proceedings of the Royal Society of London. Series A: Mathematical, Physical and Engineering Sciences* **454** (1970), 725–742.

Lötters, Joost Conrad, Olthuis, Wouter, Veltink, Petrus H & Bergveld, Piet 1997 The mechanical properties of the rubber elastic polymer polydimethylsiloxane for sensor applications. *Journal of micromechanics and microengineering* **7** (3), 145.

Lutz, Barry R, Chen, Jian & Schwartz, Daniel T 2005 Microscopic steady streaming eddies created around short cylinders in a channel: Flow visualization and stokes layer scaling. *Physics of Fluids* **17** (2), 023601.

Lutz, Barry R, Chen, Jian & Schwartz, Daniel T 2006 Hydrodynamic tweezers: 1. noncontact trapping of single cells using steady streaming microeddies. *Analytical chemistry* **78** (15), 5429–5435.

Marmottant, Philippe & Hilgenfeldt, Sascha 2004 A bubble-driven microfluidic transport element for bioengineering. *Proceedings of the National Academy of Sciences* **101** (26), 9523–9527.

MICHELL, JH 1899 On the direct determination of stress in an elastic solid, with application to the theory of plates. *Proceedings of the London Mathematical Society* **1** (1), 100–124.

RANEY, WP, CORELLI, JC & WESTERVELT, PJ 1954 Acoustical streaming in the vicinity of a cylinder. *The Journal Of The Acoustical Society of America* **26** (6), 1006–1014.

SPELMAN, TAMSIN A & LAUGA, ERIC 2017 Arbitrary axisymmetric steady streaming: Flow, force and propulsion. *Journal of Engineering Mathematics* **105** (1), 31–65.

VISHWANATHAN, GIRIDAR & JUAREZ, GABRIEL 2019 Steady streaming viscometry of newtonian liquids in microfluidic devices. *Physics of Fluids* **31** (4), 041701.

WANG, ZHIXIN, VOLINSKY, ALEX A & GALLANT, NATHAN D 2014 Crosslinking effect on polydimethylsiloxane elastic modulus measured by custom-built compression instrument. *Journal of Applied Polymer Science* **131** (22).